


Article

A Multi-Antenna Spectrum Sensing Method Based on CEEMDAN Decomposition Combined with Wavelet Packet Analysis

Suoping Li ^{1,*} , Yuzhou Han ^{1,*}, Jaafar Gaber ² , Sa Yang ¹ and Qian Yang ¹

¹ School of Electrical & Information Engineering, Lanzhou University of Technology, Lanzhou 730050, China; ys_sayang@126.com (S.Y.); ystrong4@163.com (Q.Y.)

² Department of Computer Science and Computer Engineering, Universite de Technologie Belfort-Montbéliard, 90010 Belfort, France; gaber@utbm.fr

* Correspondence: lsuop@lut.edu.cn (S.L.); 19119376252@163.com (Y.H.)

Abstract: In many practical communication environments, the presence of uncertain and hard-to-estimate noise poses significant challenges to cognitive radio spectrum sensing systems, especially when the noise distribution deviates from the Gaussian distribution. This paper introduces a cutting-edge multi-antenna spectrum sensing methodology that synergistically integrates complete ensemble empirical mode decomposition with adaptive noise (CEEMDAN), wavelet packet analysis, and differential entropy. Signal feature extraction commences by employing CEEMDAN decomposition and wavelet packet analysis to denoise signals collected by secondary antenna users. Subsequently, the differential entropy of the preprocessed signal observations serves as the feature vector for spectrum sensing. The spectrum sensing module utilizes the SVM classification algorithm for training, while incorporating elite opposition-based learning and the sparrow search algorithm with genetic variation to determine optimal kernel function parameters. Following successful training, a decision function is derived, which can obviate the need for threshold derivation present in conventional spectrum sensing methods. Experimental validation of the proposed methodology is conducted and comprehensively analyzed, conclusively demonstrating its remarkable efficacy in enhancing spectrum sensing performance.

Keywords: spectrum sensing; complete ensemble empirical mode decomposition with adaptive noise (CEEMDAN); wavelet packet analysis; improvement sparrow search algorithm; SVM classification; machine learning



Citation: Li, S.; Han, Y.; Gaber, J.; Yang, S.; Yang, Q. A Multi-Antenna Spectrum Sensing Method Based on CEEMDAN Decomposition Combined with Wavelet Packet Analysis. *Electronics* **2023**, *12*, 3823. <https://doi.org/10.3390/electronics12183823>

Academic Editor: Matteo Bruno Lodi

Received: 6 August 2023

Revised: 6 September 2023

Accepted: 7 September 2023

Published: 9 September 2023



Copyright: © 2023 by the authors. Licensee MDPI, Basel, Switzerland. This article is an open access article distributed under the terms and conditions of the Creative Commons Attribution (CC BY) license (<https://creativecommons.org/licenses/by/4.0/>).

1. Introduction

In recent years, static spectrum allocation strategies struggled to meet the growing demand for spectrum resources. Within dedicated frequency bands, substantial portions of spectrum resources remain unused, both in terms of time and frequency domains [1]. While static allocation strategies effectively manage interference among communication systems operating in separate frequency bands, they exhibit inherent inflexibility. When primary users either refrain from utilizing their allocated spectrum for extended periods or use it intermittently, these idle frequency bands become inaccessible to other radio users. To address this contradiction, Dr. Mitola proposed the concept of cognitive radio (CR) [2]. As a new wireless communication technology, CR became an ideal solution to improve spectrum utilization, and spectrum sensing plays a crucial role in CR.

Several common spectrum sensing methods were proposed in references [3–5]. The energy detection algorithm compares the received signal energy with a threshold to determine the presence of a signal [3]. The matched filter detection correlates the received signal with a known transmitted signal to detect the existence of a primary user signal [4]. The cyclostationary feature detection adjusts the number of samples involved in real time based

on changes in signal-to-noise ratio (SNR), analyzing the corresponding spectral correlation characteristics to determine the presence of a primary user [5]. Moreover, these detection methods have their limitations. The energy detection method is susceptible to interference from noise uncertainty and faces challenges in determining the decision threshold. Additionally, these detection algorithms are primarily evaluated under the assumption of additive Gaussian white noise for computational convenience.

In complex electromagnetic environments, the influence of interference and noise often follows a generalized Gaussian distribution (GGD), as observed in communication systems such as ultra-wide band (UWB) receivers [6]. At low SNR, the accuracy of spectrum sensing algorithms is diminished due to the uncertainty arising from noise. Consequently, this uncertainty affects the estimation of the signal by spectrum sensing algorithms. To address this issue, several traditional filtering denoising methods were proposed, including mean filtering, adaptive filtering, and wavelet analysis. However, these methods come with certain limitations. For instance, the effectiveness of adaptive filtering in noise suppression relies on the power spectral differences between the signal and the noise, making it less effective when the power spectra of the signal and noise are similar [7]. Empirical mode decomposition (EMD) decomposes signals into intrinsic mode functions (IMFs) without requiring the specification of wavelet basis functions. However, it struggles to handle non-stationary signals effectively [8]. Ensemble empirical mode decomposition (EEMD) was designed to address the mode mixing problem in EMD decomposition by adding white noise to the original signal for analysis [9]. Although the EEMD method solves the mixed mode problem, it is essentially a decomposition method that reduces the purity of the original signal, which will lead to the distortion of the signal. Furthermore, the residual noise introduced during decomposition contributes to increased signal reconstruction errors. To mitigate this limitation, Torres et al. introduced the complete ensemble empirical mode decomposition with adaptive noise (CEEMDAN) denoising method [10]. In the CEEMDAN method, adaptive white noise is added to each EMD stage, and its specific residual is calculated to obtain each modal component. Compared with the EEMD method, it overcomes the mode aliasing and effectively reduces the reconstruction error [11]. Although the CEEMDAN algorithm eliminates the mode aliasing and the reconstruction error is small, it will cause the loss of useful signal and incomplete echo signal in the high-frequency component.

To address the spectrum sensing problem, researchers employed machine learning classification algorithms to convert it into a binary classification problem, i.e., whether the primary user is using the licensed spectrum or not. Sarikhani et al. proposed a deep reinforcement learning method for spectrum sensing classification based on a collaborative spectrum sensing model, achieving promising results [12]. Thilina et al. adopted signal energy as a feature vector and applied the machine learning methods such as K-means, neural networks, and support vector machines (SVM), achieving effective spectrum sensing [13]. Tan et al. proposed a fusion algorithm based on random forests, incorporating sensor velocity, signal energy, and average eigenvalues of the covariance matrix as feature parameters, resulting in enhanced detection performance [14]. Wang et al. proposed a cooperative spectrum sensing method based on empirical mode decomposition and information geometry. They employed a K-medoids clustering algorithm for training in the spectrum sensing module, resulting in improved detection probability. However, under low SNR conditions, the detection probability significantly decreases [15]. Saravanan et al. used the differential entropy estimates in the received observations as feature vectors for the SVM algorithm spectrum sensing model training, but the spectrum sensing performance degrades rapidly as the shape parameter β increases [16]. Sheng et al. proposed a method to extract the trace of the covariance matrix and the quadratic covariance matrix as the combination of feature vectors for spectrum sensing training samples. They employed a genetic algorithm to optimize SVM parameters, achieving good sensing results, although the genetic algorithm optimization method is considered outdated [17].

In recent years, many scholars used heuristic algorithms to optimize the relevant parameters of machine learning algorithms, such as the sparrow search algorithm (SSA) [18]. Gao et al. used SSA to optimize the parameters of variational mode decomposition (VMD) to solve the problem that it is difficult to manually set the parameters to achieve the optimal VMD decomposition [19]. Li et al. used the sparrow search algorithm to optimize the parameters of the SVM and established a nonlinear relationship model between the melting process and technological indicators, which improved the model accuracy [20]. Qu et al. proposed a hybrid fault diagnosis method based on wavelet packet energy spectrum and SSA-SVM. The sparrow search algorithm was used to optimize the penalty factor and kernel parameters globally to improve the classification accuracy of the SVM [21]. However, the original sparrow search algorithm used in the above-related literature has the problems of low convergence accuracy, poor optimization efficiency, single search direction, and falling into local optimum.

Based on existing research, this paper proposes a multi-antenna spectrum sensing method named CEEMDAN-DE, which combines complete ensemble empirical mode decomposition with adaptive noise (CEEMDAN) decomposition and differential entropy (DE). Firstly, the signal collected by the secondary user is decomposed by CEEMDAN to obtain multiple IMF components. Then, the IMF components with high noise are screened out by calculating the correlation coefficient. Taking advantage of the fact that wavelet packet decomposition can provide more detailed signal frequency characteristics [22], the IMF component containing noise is denoised by wavelet packet analysis. Finally, the pure signal is obtained by component reconstruction. This joint noise removal method preserves the integrity and particularity of the original signal while eliminating the noise, and avoids the distortion problem and the loss of useful signals in high-frequency components caused by CEEMDAN. Finally, considering the shortcomings of the original sparrow search algorithm, the sparrow search algorithm combining elite opposition-based learning and genetic variation is established to determine the kernel function parameters of the SVM algorithm. This optimized SVM algorithm is employed for spectrum sensing. The experimental section includes the validation of the proposed method using receiver operating characteristic (ROC) curves, demonstrating its effectiveness.

The rest of this paper is organized as follows: Section 2 describes the multi-antenna spectrum sensing model and the CEEMDAN feature extraction method. Section 3 first introduces the optimization process of the sparrow search algorithm based on elite opposition-based learning and genetic variation, and then introduces the complete SVM spectrum sensing model. In Section 4, we substantiate the efficacy of the ISSA algorithm via the heuristic algorithm detection function. Then, the effectiveness of the CEEMDAN-wavelet packet analysis denoising method is verified under different SNRs. Next, the detection probability of the CEEMDAN-DE method under different SVM kernel function models is verified and compared. Under different SNRs, the superiority of the proposed method is proved by comparing the ROC curves of different feature extraction methods. Section 5 discusses the main work and contributions of this paper.

2. Multi-Antenna Spectrum Sensing in the Complex Communication Environment

In cognitive radio systems, users can be classified into two categories based on the usage priority of the licensed spectrum: primary users (PUs) and secondary users (SUs). PUs have absolute priority to use the licensed spectrum, while SUs continuously detect the presence of PUs through spectrum sensing, which ensures that SUs can access the PUs spectrum for communication tasks without causing interference with the normal communication of PUs. Therefore, an efficient and fast spectrum sensing technology is a prerequisite for building cognitive radio systems.

In comparison to single-antenna spectrum sensing, multi-antenna spectrum sensing offers numerous advantages [23]. It not only enhances detection performance by incorporating spatial information, but also reliably perceives primary user activities even in the lack of signal and noise variance information.

2.1. Spectrum Sensing Problem Model

The spectrum sensing problem is classified as a signal detection problem, the core of which is to determine whether the primary user signal exists. This can be effectively described using a binary hypothesis test:

$$\begin{cases} H_0 : \text{Primary user signal does not exist} \\ H_1 : \text{Primary user signal exists} \end{cases} \quad (1)$$

Consider a cognitive radio system consisting of a primary user with a single antenna and secondary users with M ($M > 1$) receiving antennas. The secondary users utilize their receiving antennas to detect whether the primary user is transmitting a signal. Under a binary hypothesis test, the received signals from the antennas can be represented as follows:

$$x_m(n) = \begin{cases} w_m(n), & H_0 \\ s(n) + w_m(n), & H_1 \end{cases} \quad (n = 1, 2, \dots, N). \quad (2)$$

In the scenario considered, we have two hypotheses: H_0 and H_1 . When H_0 is true, the channel solely consists of samples of noise denoted as $w_m(n)$, which follows a generalized Gaussian distribution in a complex environment. In this case, there is no presence of a primary user signal $s(n)$, and the secondary user (SU) can utilize the channel. Conversely, when H_1 holds true, the channel encompasses both noise and the primary user's signal, rendering the channel unavailable. N represents the number of observed samples.

For measuring the performance of a sensing system, common reference metrics include false alarm probability P_f and detection probability P_d . The false alarm probability P_f represents the event probability that the fusion center misjudges the presence of the primary user when the primary user does not exist.

$$P_f = \text{Prob}\{H_1|H_0\} \quad (3)$$

The detection probability P_d represents the probability that the primary user exists and is correctly detected.

$$P_d = \text{Prob}\{H_1|H_1\} \quad (4)$$

2.2. Feature Extraction Based on CEEMDAN

During the process of feature extraction, the observations collected by M ($M > 1$) receiving antennas are initially subjected to CEEMDAN combined with wavelet packet analysis for denoising, reducing noise, and redundant information in the acquired signals, thereby enhancing the overall performance of the sensing system. Subsequently, the estimated differential entropy (DE) values based on the observed data are utilized as feature vectors for signal feature extraction.

2.2.1. CEEMDAN Decomposition Principle

The EEMD and complete ensemble empirical mode decomposition (CEEMD) decomposition algorithms both address the mode mixing problem in EMD decomposition by adding Gaussian white noise or paired positive–negative Gaussian white noise to the signal to be decomposed [24]. However, neither of these algorithms isolate the residual noise, resulting in the added white noise signal being able to shift from high frequencies to low frequencies. As a result, a portion of the white noise signal remains in the decomposed intrinsic mode components, which can affect subsequent signal analysis and processing.

CEEMDAN decomposition addresses the above-mentioned issues in two aspects:

- Adding the IMF component with auxiliary noise after EMD decomposition, rather than adding Gaussian white noise directly to the original signal;
- Both EEMD and CEEMD methods employ a strategy of averaging the acquired mode components following empirical mode decomposition to tackle the mode mixing problem. However, CEEMDAN introduces a unique approach. It performs global

averaging on the first-order IMF to obtain the final first-order IMF and then iterates this process on the residual component. This innovative approach effectively addresses the issue of noise transfer from high frequencies to low frequencies.

Let E_i represent the i th IMF obtained after EMD. The i th IMF obtained through CEEM-DAN is denoted as $\overline{C_i(n)}$, where v^j represents Gaussian white noise following a standard normal distribution, ε denotes the standard deviation of the noise, and $x_m(n)$ represents the original signal received by the antenna. The steps of CEEMDAN decomposition are as follows:

A new signal $x_m(n) + (-1)^q \varepsilon v^j(n)$ is obtained by adding plus-minus pairs of Gaussian white noise to the original signal $x_m(n)$. The first order intrinsic mode component C_1 is obtained by EMD decomposition of the new signal:

$$x_m(n) + (-1)^q \varepsilon v^j(n) = C_1^j(n) + r^j, q = 1 \text{ or } 2 \tag{5}$$

Summing and averaging the resulting L modal components, the following is obtained.

$$\overline{C_1(n)} = \frac{1}{L} \sum_{j=1}^L C_1^j(n) \tag{6}$$

Calculate the residual error after removing first modal component:

$$r_1(n) = x_m(n) - \overline{C_1(n)}. \tag{7}$$

Adding pairs of positive and negative Gaussian white noise to $r_1(n)$ is a new signal; with a new signal as the carrier for the EMD decomposition, we can obtain the phase 1 modal component D_1^j , thus the available modal component phase 2:

$$\overline{C_2(n)} = \frac{1}{L} \sum_{j=1}^L D_1^j(n). \tag{8}$$

Calculate to remove the second residual modal component:

$$r_2(n) = r_1(n) - \overline{C_2(n)}. \tag{9}$$

Repeat the above steps until the obtained residual signal is a monotone function and cannot be decomposed further, and the algorithm ends. At this time, if the number of eigenmode components obtained is K , then the original signal $x_m(n)$ is decomposed into:

$$x_m(n) = \sum_{k=1}^K \overline{C_k(n)} + r_K(n). \tag{10}$$

2.2.2. Wavelet Packet Analysis of Noise Reduction Principle

Wavelet packet analysis decomposes a noisy signal into multiple sub-band signals, allowing for better separation of different frequency components. By applying noise reduction techniques to these sub-bands, it becomes possible to selectively remove noise while preserving useful information in the signal. Compared to wavelet denoising, wavelet packet analysis offers higher frequency resolution, enabling further elimination of noise residues in the high-frequency portion.

Define the subspace U_j^n to be the closure space of the function $U_n(t)$ and U_j^{2n} to be the closure space of the function $U_{2n}(t)$, such that $U_n(t)$ is satisfied,

$$\begin{cases} U_{2n+1}(t) = \sqrt{2} \sum_{K \in \mathbb{Z}} g(k) U_n(2t - k) \\ U_{2n}(t) = \sqrt{2} \sum_{K \in \mathbb{Z}} q(k) U_n(2t - k) \end{cases} \tag{11}$$

where $q(k)$ and $g(k)$ are orthogonal filter coefficients and $g(k) = (-1)^k q(1 - k)$. When $u_0 = \varnothing(t)$, the sequence constructed by Equation (11) is called an orthogonal wavelet packet.

If $g_j^n \in U_j^n$, then $g_j^n(t)$ can be expressed as:

$$g_j^n = \sum_l d_l^{j,n} U_n(2^j t - 1) \tag{12}$$

The result of wavelet packet decomposition can be obtained:

$$\begin{cases} d_l^{j,2n} = \sum_k a_{k-2l} d_k^{j+1,n} \\ d_l^{j,2n+1} = \sum_k s_{k-2l} d_k^{j+1,n} \end{cases} \tag{13}$$

Wavelet packet reconstruction for the inverse process of wavelet packet decomposition algorithm, by $\{d_l^{j,2n}\}$ and $\{d_l^{j,2n+1}\}$ construct $\{d_l^{j+1,n}\}$.

$$d_l^{j+1,n} = \sum_k (q_{l-2k} d_l^{j,2n} + g_{l-2k} d_l^{j,2n+1}) \tag{14}$$

2.2.3. CEEMDAN Decomposes Joint Wavelet Packet Analysis

As shown in Figure 1, the initial step involves utilizing the CEEMDAN algorithm to decompose the original signal into multiple intrinsic mode components. By comparing the correlation coefficient between each mode component and the original signal, the intrinsic mode components containing noise are screened out, and the spectral distribution characteristics and variance contribution rate of the intrinsic mode components are checked. Finally, the modal components containing noise are selected by wavelet packet analysis for threshold denoising, which avoids the problem that IMF components containing more noise are directly discarded, resulting in the loss of effective information. The signal $\tilde{x}_m(n)$ is obtained by reconstructing the denoised modal component and the unprocessed modal component.

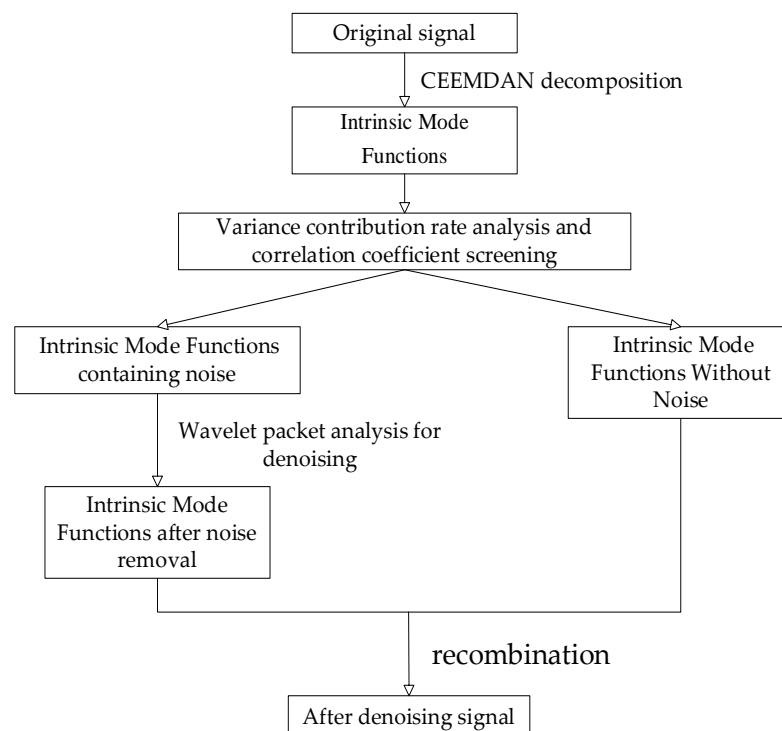


Figure 1. CEEMDAN-wavelet packet analysis joint noise reduction.

2.2.4. Feature Extraction Method Based on GGD Distribution

Generalized Gaussian noise finds relevance in various applications, including image processing, signal processing, and communication systems, among others. In these domains, signals are influenced by diverse factors, including weather-related interference, resulting in signals comprising different types and varying intensities of noise. Consequently, the noise distribution deviates from the conventional Gaussian distribution, assuming a more intricate non-Gaussian form.

If the M observed signal samples from the secondary users (SUs) are independently and identically distributed, they follow a generalized Gaussian distribution (GGD). In this distribution, the parameter α ($\alpha > 0$) controls the spread of the density function, while the parameter β ($0 < \beta \leq 2$) determines the shape [25]. The probability density function of the GGD is expressed as shown in Equation (15):

$$f_X(x) = \frac{1}{2\alpha\Gamma\left(\frac{1}{\beta}\right)} \exp\left(-\frac{|x|^\beta}{\alpha}\right), x \in \mathbb{R}. \quad (15)$$

Differential entropy (DE) is an extension of information entropy that measures the instantaneous entropy of a signal. It provides a measure of the speed of change and uncertainty in a signal. For a continuous random variable x with a probability density function $p(x)$, the DE is defined as:

$$h(X) = -\int_{-\infty}^{\infty} p(x) \ln p(x) dx. \quad (16)$$

The DE feature of samples generated from GGD noise is given by its maximum likelihood estimation [25] and can be expressed as:

$$T_{CEEMDAN-DE} = \frac{1}{\beta} - \log\left[\frac{\beta}{2\Gamma\left(\frac{1}{\beta}\right)}\right] + \frac{1}{\beta} \log\left[\frac{\beta}{N} \sum_{i=1}^N |\tilde{x}_m(n) - \hat{X}|^\beta\right] \quad (17)$$

where $0 < \beta \leq 2$ controls the “shape” of the generalized Gaussian distribution (GGD), which determines the rate of decay. \hat{X} represents the sample mean of the received observations and can be expressed as:

$$\hat{X} = \frac{1}{N} \sum_{n=1}^N \tilde{x}_m(n). \quad (18)$$

Let X be a logarithmic random variable. According to the concept of geometric moments in [26], we define the geometric moment of X as follows:

$$S_0 = S_0(X) = e^{E\{\log|X|\}}. \quad (19)$$

Suppose that $\tilde{x}_m(1), \tilde{x}_m(2), \dots, \tilde{x}_m(n)$ is an independent sample sequence from the geometric power distribution S_0 , then the statistical result can be expressed as:

$$T_{CEEMDAN-GP} = \exp\left(\frac{1}{N} \sum_{n=1}^N \log|\tilde{x}_m(n)|\right) = \left(\prod_{n=1}^N |\tilde{x}_m(n)|\right)^{1/N}. \quad (20)$$

In multi-antenna spectrum sensing, the signal samples are received by the m th secondary user’s antenna and denoted as $x_m(n)$ ($n = 1, 2, \dots, N$). Based on the feature extraction method, we compute the differential entropy and geometric power of $\tilde{x}_m(n)$. The results are denoted as $T_{CEEMDAN-DE,m}$ and $T_{CEEMDAN-GP,m}$ ($m = 1, 2, \dots, M$). Consequently, two sets of feature vectors are obtained ($T_{CEEMDAN-DE,1}, \dots, T_{CEEMDAN-DE,M}$) and ($T_{CEEMDAN-GP,1}, \dots, T_{CEEMDAN-GP,M}$). These feature vectors capture relevant information about the signal characteristics and are obtained through the CEEMDAN-DE and CEEMDAN-GP methods, respectively. They provide a comprehensive representation of the

observed signals from different antennas in the multi-antenna spectrum sensing scenario. The feature extraction process based on CEEMDAN is shown in Figure 2.

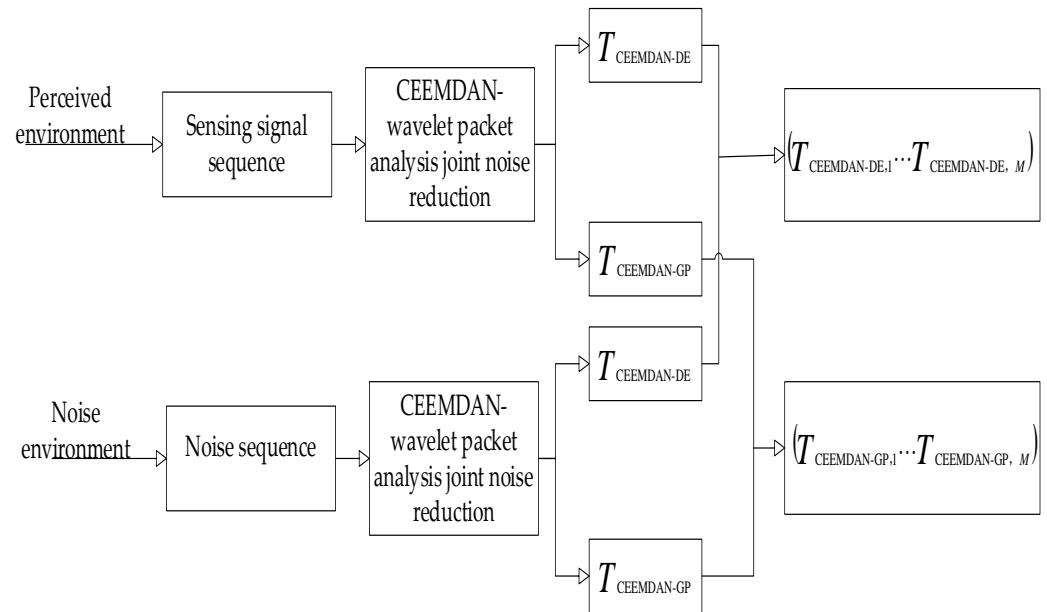


Figure 2. Feature extraction process based on CEEMDAN.

3. Multi-Antenna Spectrum Sensing Based on ISSA-SVM

3.1. Improvement Sparrow Search Algorithm

Addressing the shortcomings of the original sparrow search algorithm (SSA) [15], we propose an improved sparrow search algorithm (ISSA) based on the integration of elite opposition-based learning and genetic variation. To overcome SSA limitations, including low convergence accuracy and poor optimization efficiency, we introduce the elite opposition-based learning mechanism. Furthermore, we address the issue of SSA’s single search direction by incorporating a multi-directional learning strategy. The genetic variation strategy enhances the algorithm’s capability to escape local optima by introducing genetic variations to the local optimal individual.

Elite opposition solution definition: Let $x_i(t)$ be a solution of the t iteration, and the reverse solution is $\bar{x}_i(t)$. When $f(x_i(t)) \geq f(\bar{x}_i(t))$, $x_i(t)$ is called the elite individual of the t iteration; when $f(x_i(t)) \leq f(\bar{x}_i(t))$, $\bar{x}_i(t)$ is the elite individual of the t iteration, and x_{ij} is the value of the ordinary individual x_i on the j th dimension, then its reverse solution is

$$\bar{x}_{ij}(t) = m(l_{ij}(t) + u_{ij}(t)) - x_{ij}(t) \tag{21}$$

where m is a random number between 0 and 1, called the elite opposition coefficient. $l_{ij}(t)$ and $u_{ij}(t)$ are the minimum and maximum values of $\bar{x}_i(t)$ on the j th dimension, and $[l_{ij}, u_{ij}]$ are constructed intervals by elite groups.

In the traditional SSA, followers only learn from a single explorer in each iteration, which increases the likelihood of getting trapped in local optima and weakens the algorithm’s optimization ability. To address this issue, a multi-directional learning strategy is applied to the followers, offering relatively weaker individuals among the sparrows more opportunities to explore different regions [27]. With the improvement from the multi-directional learning strategy, the update formula for follower positions becomes as follows:

$$X_{i,j}^{t+1} = \begin{cases} Q \cdot \exp\left(\frac{X_{worst}^t - X_{i,j}^t}{i^2}\right), & i > \frac{n}{2} \\ \frac{\omega_z \cdot X_{z,j}^t + \omega_o \cdot X_{o,j}^t + \omega_b \cdot X_{b,j}^t}{\omega_z + \omega_o + \omega_b}, & \text{otherwise.} \end{cases} \tag{22}$$

The equation can be expressed as follows, where X_{ij} represents the position information of the i th sparrow in the j th dimension ($j = 1, 2, \dots, iter_{max}$), t denotes the current iteration count, Q is a random number following a normal distribution, X_{worst} represents the global worst position, and ω_z , ω_o , and ω_b represent the weights assigned to the randomly selected sparrow individuals z , o , and b .

The iterative process of SSA aims to approach the optimal individual gradually. However, if the current individual becomes the local optimum, SSA is easily trapped in local optima. To overcome this issue, the mutation operator from the genetic algorithm is introduced into ISSA. This operator mutates the optimal individual within the sparrow population, enhancing the algorithm's global search capability. Additionally, to avoid prolonged search times and emphasize the effectiveness of the mutation operator, an adaptive mutation probability is utilized in ISSA [27]. The mutation probability P_m increases with the number of iterations. This adaptive approach helps individual sparrows evade local optima during the later iterations and improves the algorithm's convergence accuracy. In ISSA, set $s = 0.5$, $d = 1$, $e = 0.03$, and $\theta = 2$.

$$P_m = e + s \left(d - \frac{iter_{max} - t}{iter_{max}} \right)^\theta \quad (23)$$

The pseudo-code of the ISSA algorithm is shown in Algorithm 1.

Algorithm 1: ISSA pseudo-code.

Input: sparrow population G , the number of producers PD , proportion of scaredy birds SD , warning value ST , the maximum iterations $iter_{max}$, $w_i \in [lb - X_i, ub - X_i]$

Output: sweet spot X_{best} , optimal value f_g

1: Initialize the population using the elite opposition-based learning strategy

2: Calculate the fitness value to find the current best individual and the worst individual

3: **While** $t < iter_{max}$

4: $R = \text{rand}(1)$

5: **for** $i = 1 : (PD * G)$

6: Update the discoverer position $X_{i,j}^t \rightarrow X_{i,j}^{t+1}$

7: **end for**

8: **for** $i = (PD * G + 1) : G$

9: Update the follower position according to Equation (22)

10: **end for**

11: **for** $i = 1 : SD$

12: Update scout position

13: **end for**

14: Calculate the mutation probability P_m , generate a random number $p = \text{rand}(1)$

15: **if** $p < P_m$

16: Mutation is performed according to $\check{X}_i \leftarrow X_i + w_i$ obtain the new sparrow position

17: **else**

18: Keep the previous sparrow position X_i

19: **end if**

20: Calculate the fitness value of the new position and the original position, and compare it

21: **if** $f(\text{new}) < f(\text{old})$

22: Preserve current position

23: **end if**

24: $t = t + 1$

25: **end while**

3.2. Spectrum Sensing Based on ISSA-SVM

Since support vector machines (SVM) have certain advantages in nonlinear data processing [28], we use the SVM algorithm for spectrum sensing. The SVM classification

problem is to find a hyperplane to maximize the classification interval on the feature space. The SVM mathematical model is as follows:

$$\begin{aligned} & \underset{w, b, \xi}{\operatorname{argmin}} \frac{1}{2} \|w\|^2 + C \sum_{i=1}^n \xi_i \\ & \text{s.t. } y_i(\omega^T x_i + b) \geq 1 - \xi_i, \xi_i \geq 0, i = 1, \dots, n \end{aligned} \quad (24)$$

where w is the normal vector of the hyperplane, C is the penalty parameter, ξ_i is the relaxation variable, x_i is the eigenvector, y_i is the result label, b is the threshold, and n is the number of samples.

Considering that spectral sensing data are often linear and indivisible, it is necessary to introduce kernel function to improve generalization ability. Therefore, the Gaussian kernel function with parameter σ is selected in this paper, and the expression is as follows:

$$K(x_1, x_2) = \exp(-\sigma \|x_1 - x_2\|^2). \quad (25)$$

When the classifier is successfully trained, the decision function is obtained according to the SVM algorithm as follows:

$$f(x) = \operatorname{sgn}\left(\sum_{i=1}^D \alpha_i^* y_i K(x_1, x_2) + b^*\right). \quad (26)$$

where $\operatorname{sgn}(\cdot)$ is a symbolic function as shown in (27) and α_i^* is a Lagrange factor. After feature extraction of the classified signal sample, it is substituted into the decision function. If $f(x) = -1$, it is considered that the primary user signal does not exist. If $f(x) = 1$, the primary user signal is considered to exist.

$$\operatorname{sgn}(x) = \begin{cases} -1, & x < 0 \\ 0, & x = 0 \\ 1, & x > 0 \end{cases} \quad (27)$$

The complete spectrum sensing algorithm is shown in Algorithm 2.

Algorithm 2: Spectrum sensing algorithm based on CEEMDAN-DE.

Input: Signal sequence $x_m(n)$, number of observed samples n , number of data sets L

Output: P_f and P_d

// CEEMDAN decomposition

1: $imf, its \leftarrow \operatorname{ceemdan}(x_m(n))$

2: **for** $i = 1 : 14$

3: Calculate the correlation coefficient of the imf and the original signal

$$CC(i) \leftarrow \operatorname{corr}(imf(i,:), x_m(n), 'type', 'Pearson')$$

4: **end for**

// wavelet denoise and reconstruct

5: **for** $i = 1 : 14$ // the imf component is selected for wavelet packet decomposition

6: $x_m(n)_{imf} = imf[i]$

7: $wpt \leftarrow \operatorname{wpdec}(x_m(n)_{imf}, 3, 'db8')$ // perform wavelet packet decomposition for each $imf[i]$, using Daubechies wavelet 'db8' and decompose 3 layers

8: $nodes = \operatorname{get}(wpt, 'tn')$

9: $N_cfs = \operatorname{length}(nodes)$

10: **for** $j = 1 : N_cfs$

11: $ysoft(:, j) \leftarrow \operatorname{wthresh}(rex3(:, j), 's', thr)$ // soft threshold processing

12: **end for**

13: $x_m(n)_{imf}(:, i) = \operatorname{sum}(ysoft, 2)$

14: **end for**

```

15:  $\tilde{x}_m(n) = \text{sum}(x_m(n)\_imf, 2) + \text{sum}(imf(:, 6 : 8), 2)$  //acquired reconstruction signal
    // feature extraction
16: for  $i = 1 : L$ 
17: A sample of  $n$  observations is randomly selected in  $\tilde{x}_m(n)$  each time
18: For  $\tilde{x}_m(n)$ ,  $\text{data}_{\text{set}}(i) = (T_{\text{CEEMDAN-DE},1}, T_{\text{CEEMDAN-DE},2})$  is obtained is obtained from
    Equation (17)
19: end
20: Divide  $\text{data}_{\text{set}}(i)$  into training sets and test sets
21: The training set is used for the SVM model parameter training, and ISSA is used to determine
    kernel function parameters  $(C, \sigma)$ 
22: The decision function (26) is obtained after successful training
23: Input the test set according to the decision function (26)
24:  $P_f$  and  $P_d$  are calculated according to Equations (3) and (4)

```

4. Simulation Results and Performance Analysis

The simulation environment for CEEMDEN-DE feature extraction is created using MATLAB2021a, and ROC curve performance analysis and ISSA algorithm verification are conducted using Python 3.8.9. The processor is an Intel(R) Core (TM) i7-8550U CPU @ 1.80 GHz processor, and the RAM is a 12 GB 64-bit computer.

4.1. ISSA Algorithm Optimization Ability Test

To assess the performance of the improved sparrow search algorithm (ISSA) and compare it with the sparrow search algorithm (SSA), we conducted performance testing using six typical benchmark functions shown in Table 1. The maximum number of iterations of the experiment $iter_{max} = 1000$, and the parameter settings [29] of the comparative experiment are shown in Table 2. The convergence curves are shown in Figures 3–5. Through the analysis of the convergence curves for functions F_1 to F_6 , it can be observed that the proposed ISSA demonstrates faster convergence speed and better global search ability compared to SSA when solving complex problems.

Table 1. Test functions.

Functions	Function Name	Dimension	Domain	Optimal Value
F_1	Sphere	30	$[-100, 100]$	0
F_2	Schwefel’s Problem 2.22	30	$[-10, 10]$	0
F_3	Ackley	30	$[-32, 32]$	0
F_4	Schwefel’s Problem 2.21	30	$[-100, 100]$	0
F_5	Griewank	30	$[-600, 600]$	0
F_6	Rastrigin	30	$[-5.12, 5.12]$	0

Table 2. Parameters setting of comparison algorithm.

Algorithm	G	PD	SD	ST
SSA	30	0.2	0.1	0.8
ISSA	30	0.2	0.1	0.8

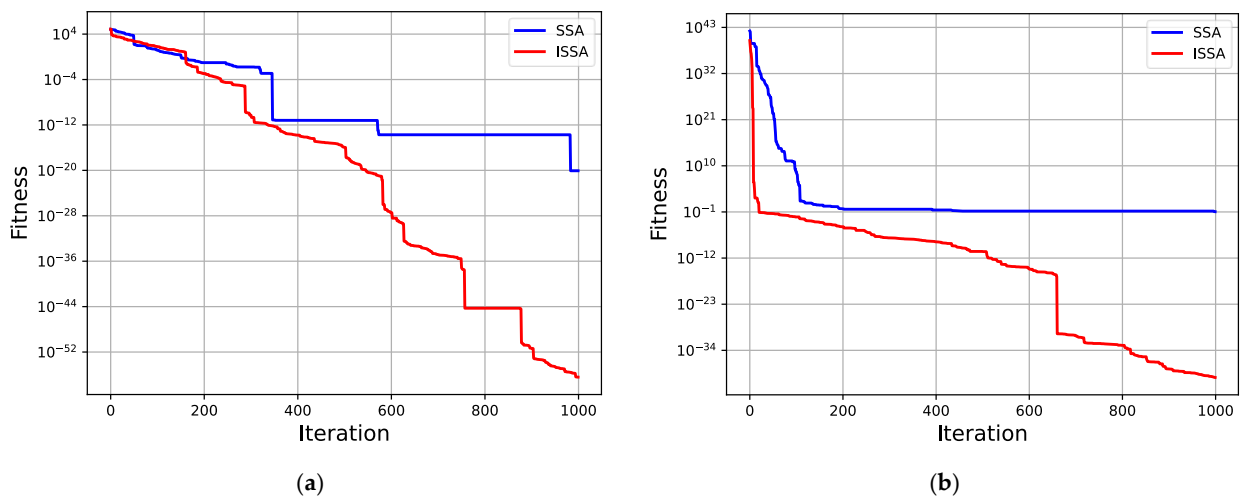


Figure 3. (a) The F_1 test function optimizes the contrast curve; (b) the F_2 test function optimizes the contrast curve.

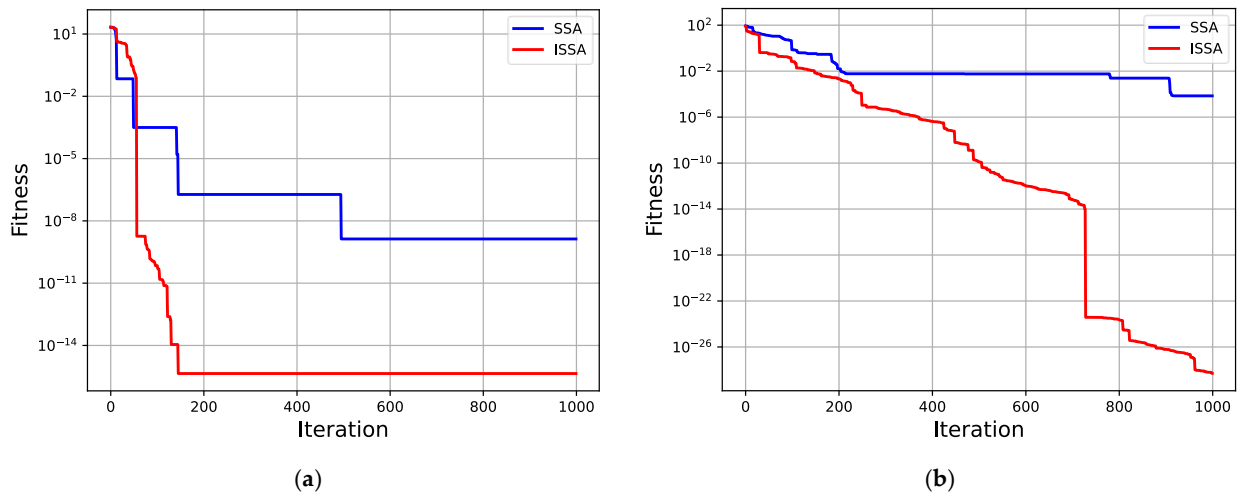


Figure 4. (a) The F_3 test function optimizes the contrast curve; (b) the F_4 test function optimizes the contrast curve.

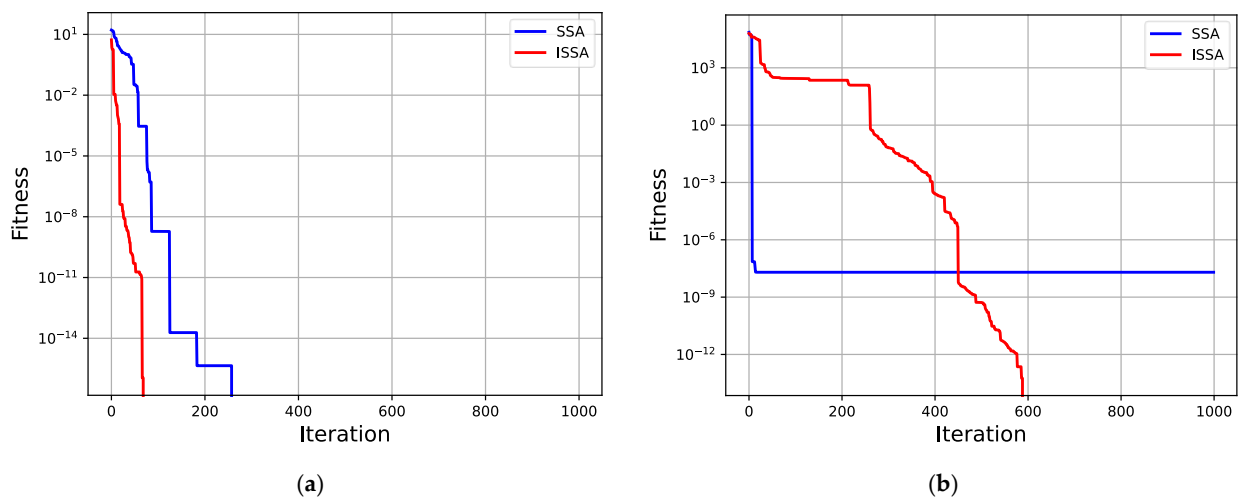


Figure 5. (a) The F_5 test function optimizes the contrast curve; (b) the F_6 test function optimizes the contrast curve.

4.2. Experimental Verification of Spectrum Sensing Method

Then, in this section, the simulated PU signal is obtained by superposition of sine and cosine functions. The simulation signal is represented as follows:

$$\begin{cases} y_1(t) = 0.35 \times \cos(0.735\pi \times 50t) \\ y_2(t) = 0.25 \times \sin(2\pi \times 50t) \times (1 + 1.5\sin(0.55\pi \times 50t)) \\ y(t) = y_1(t) + y_2(t) + w(t) \end{cases} \quad (28)$$

where $t \in [0, 2]$, the signal sampling interval $\Delta t = 2 \times 10^{-4}$ s; and $w(t)$ is the noise signal following the generalized Gaussian distribution.

The parameters related to the CEEMDAN method are set as follows: the standard deviation of the added Gaussian white noise $N_{std} = 0.2$, number of times noise is added $NR = 100$, and the maximum number of iterations $MaxIter = 500$. Simulation signal $y(t)$ is decomposed by the CEEMDAN method under different signal-to-noise ratios (SNRs).

The simulation signals of the primary users are undergoing CEEMDAN decomposition under various SNRs, yielding a series of intrinsic mode function (IMF) components ranging from high to low frequencies, as demonstrated in Table 3. The correlation coefficients among these IMF components are being calculated using the “corr” function in MATLAB. As an example, for $SNR = -12$ dB, IMF1–IMF6 components with correlation coefficients exceeding 0.2 are categorized as high-frequency components with significant noise content. Subsequently, these components undergo denoising through wavelet packet analysis. Conversely, IMF7–IMF14 components with correlation coefficients less than 0.2 are identified as low-noise components and are preserved.

Table 3. Correlation coefficient value corresponding to each order component of the primary user signal with different SNRs.

	SNR = -9 dB	SNR = -12 dB
IMF1	0.6094	0.6271
IMF2	0.4271	0.4541
IMF3	0.3465	0.3659
IMF4	0.2766	0.2907
IMF5	0.2753	0.2271
IMF6	0.2501	0.2023
IMF7	0.2203	0.1886
IMF8	0.2291	0.1881
IMF9	0.1599	0.1121
IMF10	0.0194	0.0375
IMF11	0.0366	0.0146
IMF12	0.0342	0.0161
IMF13	0.0198	0.0143
IMF14	0.0164	0.0151

Subsequently, the selected high-frequency noisy components are denoised using the wavelet packet analysis method. The denoising process utilizes the db8 wavelet basis function, a soft thresholding function, and a decomposition level of 3. After denoising, the high-frequency IMF components, now free of noise, are combined with the initially low-noise low-frequency IMF components. This reconstruction step finalizes the CEEMDAN-wavelet packet thresholding composite denoising of the primary user signal $y(t)$.

In order to more fully reflect the difference of the primary user signal $y(t)$ before and after noise reduction, two indicators of continuous mean square error and signal-to-noise ratio are introduced to evaluate the signal after noise reduction.

- Root mean squared error (RMSE): in the signal noise reduction metric, the root mean square error is defined as the expected value of the squared difference between the un-denoised signal and the denoised signal recalculated as shown in Equation (29).

$$\text{RMSE} = \sqrt{\frac{1}{N} \sum_{i=1}^N [y_i(t) - y_i^*(t)]^2} \quad (i = 1, 2, \dots, n) \quad (29)$$

- SNR: The signal-to-noise ratio is defined as shown in Equation (30).

$$\text{SNR} = 10 \times \lg \left[\frac{\sum_{i=1}^N y_i(t)^2}{\sum_{i=1}^N [y_i(t) - y_i^*(t)]^2} \right] \text{ (dB)} \quad (30)$$

where $y_i^*(t)$ is the denoised signal and n is the signal length.

To comprehensively demonstrate the superiority of the CEEMDAN-wavelet packet analysis denoising method, we conducted a comparative analysis, contrasting the performance of the proposed method with that of the EMD-wavelet packet analysis denoising and conventional EEMD denoising methods across various SNRs. The denoising efficacy for both methods is evaluated using the RMSE and SNR.

In the wavelet packet threshold denoising experiment, db8 wavelet basis function and soft threshold function are used again, and the decomposition level is still set to 3.

From the comparative results in Table 4 and the evaluation criteria for denoising performance, it is evident that the proposed CEEMDAN-wavelet packet analysis-combined denoising method outperforms both the EMD-wavelet packet analysis-combined denoising method and the EEMD denoising method for the primary user signal. Additionally, the RMSE values for the CEEMDAN-wavelet packet analysis method are consistently lower than those of the other two methods. Moreover, the SNR achieved by the CEEMDAN-wavelet packet analysis-combined denoising method is notably higher than that achieved by the other two methods.

Table 4. Performance indicators of different noise reduction methods.

Initial SNR	Evaluation Index	EMD-Wavelet Packet Analysis-Combined Denoising	EEMD	CEEMDAN-Wavelet Packet Analysis-Combined Denoising
SNR = −9 dB	RMSE	0.2383	0.2807	0.1968
	SNR/dB	3.532	2.1095	4.9743
SNR = −12 dB	RMSE	0.3154	0.3039	0.2644
	SNR/dB	1.0987	1.4289	2.6297

In the training of the spectrum sensing module using the SVM classification algorithm, as presented in literature [13] and literature [16], only the “linear” and “polynomial” kernel functions are considered. Regrettably, the more appropriate “RBF” kernel function, which is well suited for addressing nonlinear classification problems, is overlooked. These methods are denoted as linear-SVM, poly-SVM, and RBF-SVM, respectively. It is noteworthy that the “RBF” kernel function introduces an element of uncertainty due to the random generation of penalty factors C and kernel function parameters σ during each training session. Therefore, the improved sparrow search algorithm (ISSA) is used to optimize the RBF kernel parameters C and σ , which are referred to as ISSA-SVM. To comprehensively showcase the superiority of the CEEMDAN-DE-ISSA-SVM algorithm in spectrum sensing classification, it is compared with two methods from the literature.

During the simulation, the parameters are configured as follows: $\beta = 1.8$ and $\alpha = 5.2$, where α controlled the SNR of the generated signals. Each training sample consisted of $N = 100$ sampling points from the secondary user’s received signal. The chosen signal feature extraction methods encompassed CEEMDAN-DE and DE [16]. Based on the size of the generated data set, the average training time of the machine-learning-based multi-antenna spectrum sensing methods is presented in Table 5. Among the data samples, normalization is performed and 50% is selected as the training set for the SVM model and

the remaining 50% as the test set for the SVM model. The relevant parameter settings when the ISSA algorithm optimizes the SVM kernel function are shown in Table 6.

Table 5. Comparison of SVM kernel function models under different feature extraction methods when SNR = −16 dB.

Kernel Function Model Category	Experimental Data Set Size	Training Time (s)	$(P_d P_f = 0.1)$	Accuracy Rate
CEEMDAN-DE-linear-SVM	2000	0.562337	0.934	0.90
	3000	0.499887	0.952	0.91
CEEMDAN-DE-poly-SVM	2000	3.821829	0.936	0.931
	3000	3.401949	0.955	0.937
CEEMDAN-DE-ISSA-SVM	2000	0.859216	0.94	0.93225
	3000	0.796324	0.96	0.9405
DE-linear-SVM	2000	1.031003	0.09	0.7545
	3000	1.327854	0.125	0.68925
DE -poly-SVM	2000	17.339349	0.006	0.7545
	3000	15.206200	0.02	0.68925
DE-ISSA-SVM	2000	1.577460	0.79	0.83575
	3000	2.152244	0.696	0.769

Table 6. ISSA related parameter settings.

G	$iter_{max}$	Warning Value	PD	SD
30	30	0.6	0.7	0.2

As can be seen from Table 5, among the three different kernel functions, the training time of the CEEMDAN-DE-SVM model under various data sets is shorter than that of the DE-SVM model in the literature. This observation validates that the proposed denoising method in this paper aids SVM in swiftly identifying an appropriate hyperplane for data partitioning. Moreover, it is observable that the “linear” and “polynomial” kernel functions result in low detection probabilities P_d when applied to small and non-denoised data sets. In contrast, ISSA-SVM maintains normal detection probabilities even in such cases.

Among the three kernel functions of the CEEMDAN-DE-SVM model, CEEMDAN-DE-poly-SVM has the longest training time and CEEMDAN-DE-Linear-SVM has the shortest training time, but the detection probability is low. The CEEMDAN-DE-ISSA-SVM algorithm has the highest classification accuracy and detection probability. Its increased computational complexity is offset by its superior classification accuracy and detection probability. Then, under the same α and N conditions, we analyzed and compared the impact of β change on the detection probability.

We then proceeded to extract 2000 signal features using the CEEMDAN-DE feature extraction method and conducted a comparative analysis of the detection probabilities between the ISSA-SVM and RBF-SVM algorithms. This analysis is performed under various β conditions while keeping α and N constant. As shown in Table 7, the detection probability of the RBF-SVM algorithm is significantly lower than that of the ISSA-SVM under different β . It can be found that the suitability of C and σ values have a great impact on the detection probability performance of the SVM spectrum sensing model.

Table 7. Comparison of detection probability between ISSA-SVM and RBF-SVM under different β .

Model Category	β	$(P_d P_f = 0.1)$	Penalty Factors (C)	Kernel Function Parameters (σ)
ISSA-SVM	0.8	0.963	5.20779748	4.23560914
	1	0.969	0.01	4.08559084
	1.5	0.939	0.87150995	0.08230669
	2	0.893	0.10625931	0.90453521
RBF-SVM	0.8	0.961	11.0	10.5030644
	1	0.871	11.0	10.5069423
	1.5	0.869	11.0	10.4894858
	2	0.734	11.0	10.4988999

All the subsequent experiments are implemented based on the ISSA-SVM, and the relevant parameters of the ISSA algorithm are shown in Table 6. To ensure the accuracy of the experiment, we obtained 2000 signal features based on the CEEMDAN-DE feature extraction method and normalized them, among which, 1000 are used as the training set and 1000 are used as the test set. A test set is used to verify the spectrum sensing performance of the proposed method.

ROC curves are used to compare the performance of different feature extraction methods. Among them, DE and GP represent the feature extraction methods mentioned in references [16,26]. EMD-DE and EMD-GP denote the feature extraction method using the EMD-joint wavelet packet analysis denoising method, and ED is the energy detection algorithm.

Figure 6 shows the ROC curves of different feature extraction methods when $M = 2$, $\beta = 0.8$, $\alpha = 1$, and the number of sampling points $N = 25$ for each training sample of the secondary user’s received signal. As indicated in Table 8, it can be observed that the detection probability based on the CEEMDAN-DE algorithm, at $P_f = 0.1$, the CEEMDAN-DE method improved by 355% compared to the original DE method, and by 95% compared to the GP method. It can be observed that, under the same N , the multi-antenna spectrum sensing algorithm based on SVM with the CEEMDAN-DE feature extraction method proposed in this paper achieves the best performance.

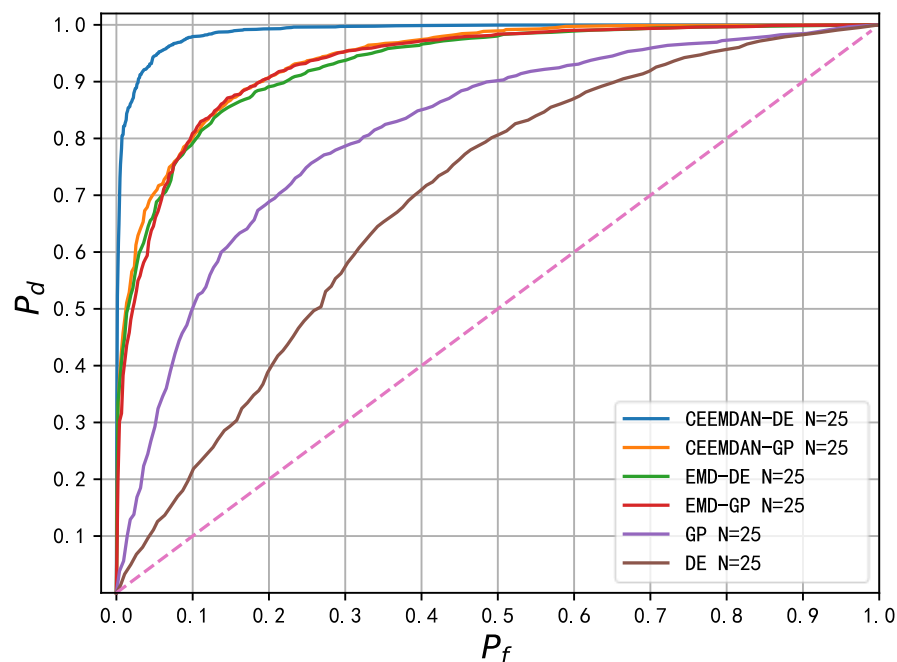


Figure 6. ROC curves of different feature extraction methods at SNR = −9 dB.

Table 8. AUC and P_d values of each feature extraction method when SNR = −9 dB.

Algorithms	AUC	$(P_d P_f = 0.1)$	Penalty Factors (C)	Kernel Function Parameters (σ)
CEEMDAN-DE	0.947461	0.979	0.05019098	0.35761508
CEEMDAN-GP	0.830064	0.801	0.28540171	0.88132311
EMD-DE	0.834399	0.791	0.94971281	1.63474901
EMD-GP	0.862792	0.809	6.96336871	0.67814947
DE	0.666286	0.215	6.94563624	6.78160817
GP	0.773780	0.501	4.98229443	5.49424544

Figure 7 illustrates the classification results obtained through feature extraction using CEEMDAN-DE. The red “+” symbols represent the feature vectors corresponding to the presence of primary user signals, while the blue “o” symbols represent feature vectors corresponding to the absence of primary user signals. The black curve represents the classification hyperplane derived after training the SVM. It is evident that the classification hyperplane successfully separates the samples into two distinct categories, with only a small number of overlapping data points.

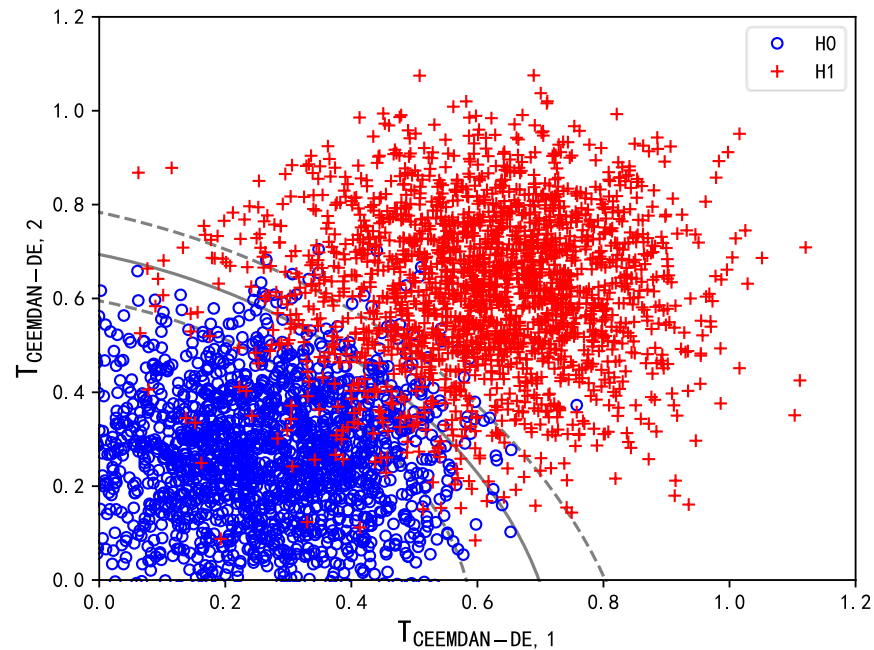


Figure 7. Classification effect diagram.

Figure 8 shows the ROC curves for different feature extraction methods when $M = 2$, $\beta = 1.7$, $\alpha = 3.2$, SNR = −14 dB, and $N = 100$. As indicated in Table 9, it can be observed that the detection probability based on the CEEDMAN-DE algorithm, at $P_f = 0.1$, exhibits a significant improvement compared to the performance of the DE method mentioned in the literature, with an increase of 588%. Furthermore, compared to the EMD-DE method, the CEEDMAN-DE algorithm demonstrates a performance improvement of 17%. It can be observed that the spectrum sensing algorithms based on DE and GP mentioned in the literature significantly decrease the spectrum sensing performance when $1 < \beta < 2$, but the method proposed in this paper can still maintain a high spectrum sensing performance.

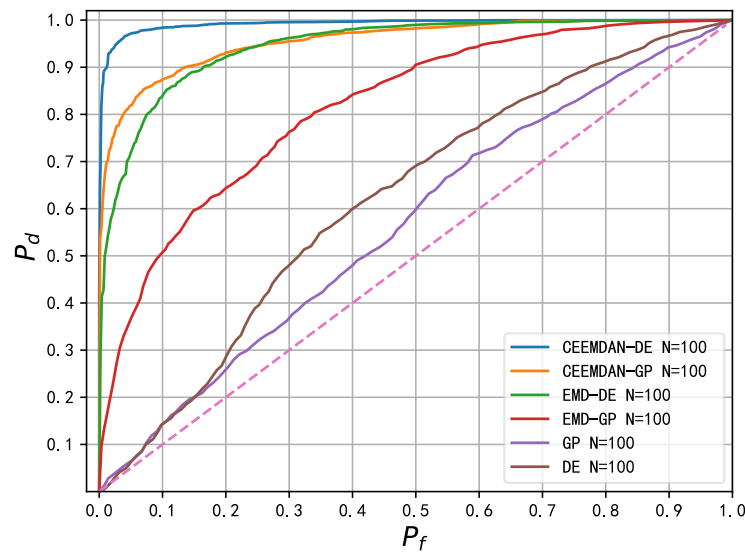


Figure 8. ROC curves of different feature extraction methods at SNR = −14 dB.

Table 9. AUC and P_d values of each feature extraction method when SNR = −14 dB.

Algorithms	AUC	$(P_d P_f = 0.1)$	Penalty Factors (C)	Kernel Function Parameters (σ)
CEEMDAN-DE	0.962633	0.9839	5.00939943	10
CEEMDAN-GP	0.882664	0.874	8.230381791	9.5211308
EMD-DE	0.871692	0.839	0.29243504	6.28011474
EMD-GP	0.679500	0.507	2.59337523	1.24635901
DE	0.540575	0.143	5.92915985	5.31179191
GP	0.507679	0.1435	9.83149123	9.78577177

In Table 10, we compare the classification performance of the ISSA-SVM spectrum sensing algorithm with K-means, decision tree, and random forest spectrum sensing algorithms when SNR = −16 dB. The metrics are area under the curve (AUC) and classification accuracy rate. Where AUC is the area under the ROC curve, which is used to measure the performance of a classifier. A higher AUC value indicates better performance of the classifier, while a lower AUC value indicates poorer performance.

Table 10. Classification performance comparison of spectrum sensing algorithms when SNR = −16 dB.

Spectrum Sensing Algorithm	β	AUC	Accuracy Rate
ISSA-SVM	0.8	0.911871	0.93225
	1.5	0.918863	0.90075
Random forest	0.8	0.907170	0.924
	1.5	0.814999	0.789
K-means	0.8	0.600418	0.495
	1.5	0.677811	0.7595
Decision tree	0.8	0.88972	0.907
	1.5	0.799265	0.77025

We can see from Table 10 that the ISSA-SVM spectrum sensing algorithm can maintain the highest classification performance regardless of $0 < \beta < 1$ or $1 < \beta < 2$. Other algorithms, such as the K-means algorithm, even fail in classification performance.

Figure 9 presents the ROC curves for the SVM-based multi-antenna spectrum sensing method under generalized Gaussian distribution noise, with varying numbers of sampling

points N . As shown in the figure, under the conditions of $M = 2$, $\beta = 0.8$, and $\alpha = 1$, with an increase in the number of sampling points N for the secondary user, the spectral sensing performance of all algorithms exhibits noticeable improvement. However, the performance of these algorithms remains lower than that of the CEEDMAN-DE method proposed in this study. This validates the effectiveness of the proposed method in scenarios with a small number of sampling points.

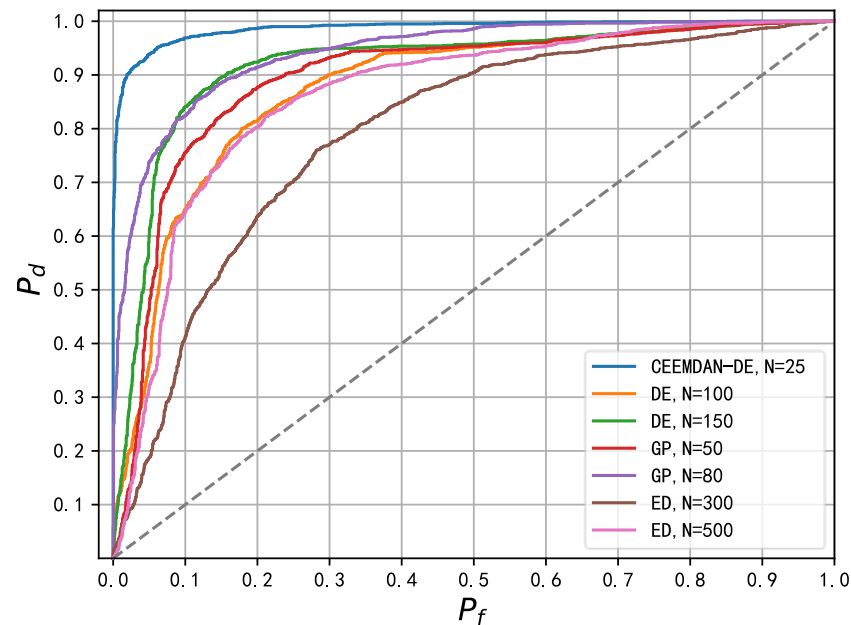


Figure 9. ROC curves for different number of sampling points N .

5. Conclusions

This paper proposes a CEEDMAN-DE method to effectively improve spectrum sensing performance in complex electromagnetic environments. In terms of feature extraction, the proposed method first utilizes CEMMDAN decomposition combined with wavelet packet analysis to denoise the signals collected by the secondary user (SU). This process enables finer removal of noise components and avoids the loss of primary user information. Then, the denoised signals are subjected to differential entropy feature extraction to obtain features for spectrum sensing. Finally, in the spectrum sensing module, the SVM classification algorithm is employed for training, combined with elite opposition-based learning and a sparrow search algorithm with genetic variation, to determine the optimal kernel function parameters. In the experiments, the performance of the CEEDMAN-DE algorithm is validated and analyzed through ROC curve analysis. When $0 < \beta < 1$, the proposed method ensures accurate spectrum sensing even with a small value of N , outperforming the spectrum sensing methods in the literature. Moreover, when $1 < \beta \leq 2$ the performance of the spectrum sensing methods in the literature deteriorates, the CEEDMAN-DE algorithm maintains accurate spectrum sensing classification. In our future work, we plan to explore a spectrum sensing algorithm that combines CEEMDAN-DE feature extraction with deep learning techniques. Additionally, we aim to investigate methods for reducing algorithmic complexity to achieve more efficient spectrum sensing.

Author Contributions: Y.H. researched the literatures, provided the mathematical models, designed the algorithm, completed numerical simulations, took charge of the original draft preparation, and edited the manuscript; S.L. conceived the study concepts, improved the systematic research and analysis methodology, and supervised the completion of the refinement of the paper; J.G., S.Y. and Q.Y. gave valuable suggestions for revision, checked formula deducing and English grammar. All authors have read and agreed to the published version of the manuscript.

Funding: This research was funded in part by the National Natural Science Foundation of China (61663024), in part by the Hongliu First Class Discipline Development Project of Lanzhou University of Technology (25–225305).

Data Availability Statement: The data supporting this article are from previously reported studies and datasets, which have been cited.

Conflicts of Interest: The authors declare no conflict of interest.

References

1. Joykutti, A.M.; Baranidharan, B. Cognitive Radio Networks: Recent Advances in Spectrum Sensing Techniques and Security. In Proceedings of the 2020 International Conference on Smart Electronics and Communication, Trichy, India, 10–12 September 2020. [\[CrossRef\]](#)
2. Mitola, J. The Software Radio Architecture. *IEEE Commun. Mag.* **1995**, *33*, 26–38. [\[CrossRef\]](#)
3. Bhavana, B.; Sabat, S.L.; Namburu, S.; Panigrahi, T. Energy Detector for Spectrum Sensing Using Robust Statistics in Non-Gaussian Noise Environment. In Proceedings of the 2023 15th International Conference on Communication Systems & Networks, Bangalore, India, 3–8 January 2023. [\[CrossRef\]](#)
4. Kumar, R.V.R. Performance Analysis of a Novel Matched Filter Detector with Reduced out-of-Band Response for Narrowband Signals. *IEEE Trans. Signal Process.* **2006**, *54*, 2691–2703. [\[CrossRef\]](#)
5. Sepidband, P.; Entesari, K. A CMOS Spectrum Sensor Based on Quasi-Cyclostationary Feature Detection for Cognitive Radios. *IEEE Trans. Microw. Theory Tech.* **2015**, *63*, 4098–4109. [\[CrossRef\]](#)
6. Ahmed, Q.Z.; Park, K.H.; Alouini, M.S. Ultrawide Bandwidth Receiver Based on a Multivariate Generalized Gaussian Distribution. *IEEE Trans. Wirel. Commun.* **2014**, *14*, 1800–1810. [\[CrossRef\]](#)
7. Habibi, Z.; Zayyani, H. Markovian Adaptive Filtering Algorithm for Block-Sparse System Identification. *IEEE Trans. Circuits Syst. II Express Briefs* **2021**, *68*, 3032–3036. [\[CrossRef\]](#)
8. Wang, Y.H.; Cheng, S.H. Boundary Effects for EMD-Based Algorithms. *IEEE Signal Process. Lett.* **2022**, *29*, 1032–1036. [\[CrossRef\]](#)
9. Xue, W.; Dai, X.; Zhu, J.; Luo, Y.; Yang, Y. A Noise Suppression Method of Ground Penetrating Radar Based on EEMD and Permutation Entropy. *IEEE Geosci. Remote Sens. Lett.* **2019**, *16*, 1625–1629. [\[CrossRef\]](#)
10. Torres, M.E.; Colominas, M.A.; Schlotthauer, G.; Flandrin, P. A Complete Ensemble Empirical Mode Decomposition with Adaptive Noise. In Proceedings of the 2011 IEEE International Conference on Acoustics, Speech and Signal Processing, Prague, Czech Republic, 22–27 May 2011. [\[CrossRef\]](#)
11. He, C.; Niu, P.; Yang, R.; Wang, C.; Li, Z.; Li, H. Incipient Rolling Element Bearing Weak Fault Feature Extraction Based on Adaptive Second-order Stochastic Resonance Incorporated by Mode Decomposition. *Measurement* **2019**, *145*, 687–701. [\[CrossRef\]](#)
12. Sarikhani, R.; Keynia, F. Cooperative Spectrum Sensing Meets Machine Learning: Deep Reinforcement Learning Approach. *IEEE Commun. Lett.* **2020**, *24*, 1459–1462. [\[CrossRef\]](#)
13. Thilina, K.M.; Choi, K.W.; Saquib, N.; Hossain, E. Machine Learning Techniques for Cooperative Spectrum Sensing in Cognitive Radio Networks. *IEEE J. Sel. Areas Commun.* **2013**, *32*, 2209–2221. [\[CrossRef\]](#)
14. Tan, C.; Chen, J.; Chen, S.; Li, C.; Liu, H.; Zheng, M. Combination Spectrum Sensing Algorithm for Wireless Sensor Network Based on Random Forest. In Proceedings of the 2022 10th International Conference on Intelligent Computing and Wireless Optical Communications, Chongqing, China, 10–12 June 2022. [\[CrossRef\]](#)
15. Wang, Y.; Zhang, S.; Zhang, Y.; Wan, P.; Li, J.; Li, N. A Cooperative Spectrum Sensing Method Based on Empirical Mode Decomposition and Information Geometry in Complex Electromagnetic Environment. *Complexity* **2019**, *2019*, 15. [\[CrossRef\]](#)
16. Saravanan, P.; Chandra, S.S.; Upadhye, A.; Gurugopinath, S. A Supervised Learning Approach for Differential Entropy Feature-based Spectrum Sensing. In Proceedings of the 2021 Sixth International Conference on Wireless Communications, Signal Processing and Networking, Chennai, India, 25–27 March 2021. [\[CrossRef\]](#)
17. Sheng, J.; Liu, F.; Zhang, Z.; Huang, C. TCVMQ-SVM Algorithm for Narrowband Spectrum Sensing. *Phys. Commun.* **2022**, *50*, 101502. [\[CrossRef\]](#)
18. Xue, J.; Shen, B. A Novel Swarm Intelligence Optimization Approach: Sparrow Search Algorithm. *Syst. Sci. Control Eng.* **2020**, *8*, 22–34. [\[CrossRef\]](#)
19. Gao, X.; Guo, W.; Mei, C.; Sha, J.; Guo, Y.; Sun, H. Short-term Wind Power Forecasting Based on SSA-VMD-LSTM. *Energy Rep.* **2023**, *9*, 335–344. [\[CrossRef\]](#)
20. Li, X.; Yang, C.; Zhang, X.; Li, G. Prediction of Matte Grade in The Oxygen-rich Top Blown Smelting Based on WD-SSA-SVM Algorithm. In Proceedings of the 2023 IEEE 12th Data Driven Control and Learning Systems Conference, Xiangtan, China, 12–14 May 2023. [\[CrossRef\]](#)
21. Qu, J.; Ma, B.; Ma, X.; Wang, M. Hybrid Fault Diagnosis Method based on Wavelet Packet Energy Spectrum and SSA-SVM. *Int. J. Adv. Comput. Sci. Appl.* **2022**, *13*, 52–60. [\[CrossRef\]](#)
22. Li, L.; Wang, F.; Shang, F.; Jia, Y.; Zhao, C.; Kong, D. Energy Spectrum Analysis of Blast Waves Based on an Improved Hilbert-Huang Transform. *Shock Waves* **2017**, *27*, 487–494. [\[CrossRef\]](#)
23. Liu, M.; Zhang, X.; Chen, Y.; Tan, H. Multi-antenna Intelligent Spectrum Sensing in The Presence of Non-Gaussian Interference. *Digit. Signal Process.* **2023**, *140*, 104135. [\[CrossRef\]](#)

24. Yeh, J.R.; Shieh, J.S.; Huang, N.E. Complementary Ensemble Empirical Mode Decomposition: A Novel Noise Enhanced Data Analysis Method. *Adv. Adapt. Data Anal.* **2010**, *2*, 135–156. [[CrossRef](#)]
25. Gurugopinath, S.; Muralishankar, R.; Shankar, H.N. Differential Entropy-Driven Spectrum Sensing Under Generalized Gaussian Noise. *IEEE Commun. Lett.* **2016**, *20*, 1321–1324. [[CrossRef](#)]
26. Gonzalez, J.G.; Paredes, J.L.; Arce, G.R. Zero-Order Statistics: A Mathematical Framework for the Processing and Characterization of Very Impulsive Signals. *IEEE Trans. Signal Process.* **2006**, *54*, 3839–3851. [[CrossRef](#)]
27. Chai, Y.; Sun, X.; Ren, S. Chaotic Sparrow Search Algorithm Based on Multi-Directional Learning. *Comput. Eng. Appl.* **2023**, *59*, 81–91. [[CrossRef](#)]
28. Akram, Z.; Fernández, M.; Cernadas, E.; Barro, S. Fast Support Vector Classification for Large-Scale Problems. *IEEE Trans. Pattern Anal. Mach. Intell.* **2021**, *44*, 6184–6195. [[CrossRef](#)] [[PubMed](#)]
29. Li, Z.; Guo, J.; Gao, X.; Yang, X.; He, Y.L. A Multi-strategy Improved Sparrow Search Algorithm of Large-scale Refrigeration System: Optimal Loading Distribution of Chillers. *Appl. Energy* **2023**, *349*, 121623. [[CrossRef](#)]

Disclaimer/Publisher’s Note: The statements, opinions and data contained in all publications are solely those of the individual author(s) and contributor(s) and not of MDPI and/or the editor(s). MDPI and/or the editor(s) disclaim responsibility for any injury to people or property resulting from any ideas, methods, instructions or products referred to in the content.